

# Boxing Day Surprise: Higher Multipoles and Orbital Precession in GW151226

Horng Sheng Chia,<sup>1,\*</sup> Seth Olsen,<sup>2</sup> Javier Roulet,<sup>2</sup> Liang Dai,<sup>3</sup>  
Tejaswi Venumadhav,<sup>4,5</sup> Barak Zackay,<sup>6</sup> and Matias Zaldarriaga<sup>1</sup>

<sup>1</sup>*School of Natural Sciences, Institute for Advanced Study, Princeton, NJ 08540, USA*

<sup>2</sup>*Department of Physics, Princeton University, Princeton, NJ 08540, USA*

<sup>3</sup>*Department of Physics, University of California, Berkeley, 366 LeConte Hall, Berkeley, CA 94720, USA*

<sup>4</sup>*Department of Physics, University of California at Santa Barbara, Santa Barbara, CA 93106, USA*

<sup>5</sup>*International Centre for Theoretical Sciences, Tata Institute of Fundamental Research, Bangalore 560089, India*

<sup>6</sup>*Dept. of Particle Physics & Astrophysics, Weizmann Institute of Science, Rehovot 76100, Israel*

We present a reanalysis of GW151226, the second binary black hole merger discovered by the LIGO-Virgo Collaboration. Previous analysis showed that the best-fit waveform for this event corresponded to the merger of a  $\sim 14 M_{\odot}$  black hole with a  $\sim 7.5 M_{\odot}$  companion. In this work, we perform parameter estimation using a waveform model that includes the effects of orbital precession and higher-order radiative multipoles, and find that the mass and spin parameters of GW151226 have bimodal posterior distributions. The two modes are separated in mass ratio,  $q$ : the high- $q$  mode ( $0.4 \lesssim q < 1$ ) is consistent with the results reported in the literature. On the other hand, the low- $q$  mode ( $q \lesssim 0.4$ ), which describes a binary with component masses of  $\sim 29 M_{\odot}$  and  $\sim 4.3 M_{\odot}$ , is new. The low- $q$  mode has several interesting properties: (a) the secondary black hole mass may fall in the lower mass gap of astrophysical black hole population; and (b) orbital precession is driven by the primary black hole spin, which has a dimensionless magnitude as large as  $\sim 0.88$  and is tilted away from the orbital angular momentum at an angle of  $\sim 47^{\circ}$ . The new low- $q$  mode has a log likelihood that is about six points higher than that of the high- $q$  mode, and can therefore affect the astrophysical interpretation of GW151226. Crucially, we show that the low- $q$  mode disappears if we neglect either higher multipoles or orbital precession in the parameter estimation. More generally, this work highlights how incorporating additional physical effects into waveform models used in parameter estimations can alter the interpretation of gravitational-wave sources.

## I. INTRODUCTION

GW151226 was one of the earliest confident binary black hole mergers detected by the LIGO–Virgo Collaboration (LVC) [1, 2]. This event, identified on December 26 2015, is interesting because it is a low-mass binary system and was consequently observed over a large number of cycles ( $\sim 55$ ) in the detector sensitive bands. The large number of cycles allows us to characterize the signal relatively precisely and helps us draw more detailed conclusions about the underlying system. For example, one of the black holes was inferred to have non-vanishing spin along the direction of the orbital angular momentum, at  $\gtrsim 90\%$  confidence [1–5]. These measurements, in turn, provide important constraints on astrophysical formation channels for binary black holes [6, 7] and enable tests of General Relativity in the strong-gravity regime [8, 9].

While the astrophysical implications of GW151226 have been extensively explored in the literature, those works relied on source parameters that were inferred using waveform models that exclude either orbital precession, higher-order radiative multipoles, or both. For instance, the parameter estimations conducted in Refs. [3, 4] and the base results in the official LVC papers [1, 2] utilized waveform models that assume the spins of the

black holes are aligned with the orbital angular momentum, and only include the dominant quadrupolar radiation [10–12]. The LVC [1, 2] and the independent PyCBC group [5] also presented analyses with waveform models that incorporate orbital precession, but exclude higher multipoles [13–15]. In contrast, Ref. [16] used the likelihood reweighting method [17, 18] to reanalyze GW151226 with a waveform model that includes higher multipoles but not precession [19]. The results of those studies were broadly consistent with one another, and found no significant signs of either higher multipoles or orbital precession in GW151226.

Recent advancements in template waveform modeling have led to the construction of models that encapsulate *both* precession and higher multipoles in a unified framework [20–23]. To the best of our knowledge, these state-of-the-art models have not been used to re-analyze GW151226, or more broadly, the larger set of events identified in the first and second LVC observing runs (O1 and O2). For instance, in their latest population analysis paper [24], the LVC used the posterior samples derived with the older waveform models [12–15] for the O1 and O2 events, although new models which include precession and higher multipoles are used to analyze the events identified in the first half of the third observing run (O3a) [21–23].

In this work, we reanalyze GW151226 using IMRPhenomXPHM [20], a recently-developed waveform model which includes both higher multipoles and the ef-

\* [hschia@ias.edu](mailto:hschia@ias.edu)

fects of orbital precession in the gravitational waveforms for quasi-circular binary black hole mergers. Remarkably, we find that the posterior distributions of the source parameters of GW151226 in this work are bimodal. The two modes in the posterior distributions are separated in mass ratio, which we define as  $q \equiv m_2/m_1 \leq 1$ , where  $m_1$  and  $m_2$  are the primary and secondary masses of the binary black holes, respectively. The high- $q$  mode, with  $0.4 \lesssim q < 1$ , has source parameters that are consistent with the results reported in earlier studies [1–5]. On the other hand, the low- $q$  mode, with  $q \lesssim 0.4$ , is new and has a log likelihood that is about six points larger than that of the high- $q$  mode. Crucially, as we shall demonstrate, the low- $q$  mode would disappear when either higher multipoles or orbital precession is disabled in the parameter estimation process. This observation highlights the importance of both of these physical effects for the emergence of the newfound solution, and offers a compelling explanation as to why it had not been reported in the literature.

In addition to having a small mass ratio and displaying signs of precession, the low- $q$  mode is qualitatively distinct from the high- $q$  mode for a variety of reasons. Firstly, the secondary source mass of the new solution has a median and 90% symmetric credible interval of  $m_2 = 4.3_{-0.8}^{+1.7} M_\odot$ , making it a potential candidate that falls in the hypothesized lower mass gap of black hole populations, which is roughly at  $2.5\text{--}5 M_\odot$  [25–27]. Secondly, the primary black hole of the low- $q$  mode is found to have a very large spin magnitude,  $|\vec{\chi}_1| = 0.88_{-0.14}^{+0.11}$ , one which is in fact close to extremality. Furthermore, we find that the primary spin is tilted away from the orbital angular momentum at  $\theta_{1L} = (47_{-18}^{+15})^\circ$  and is therefore the main driver of precession. The secondary spin, on the other hand, is unconstrained. Since these source properties are drastically different from those of the high- $q$  mode [1–5], GW151226 could be a binary system that is entirely different from what was previously inferred. The emergence of this new solution also serves to motivate further advancements in the waveform modeling frontier, such that the source properties of current and future detected binary signals could be accurately determined.

This paper is organized as follows: in Section II, we describe our parameter estimation method, and outline the different setups that we design in order to decipher the underlying physics of GW151226. In Section III, we report the parameter estimation results. In Section IV, we elaborate on our findings, and show that the conclusions drawn for the primary spin of the low- $q$  mode remains unchanged when a different spin prior is adopted. In Section V, we discuss the astrophysical implication of the low- $q$  mode. Finally, we summarize and conclude in Section VI. In Appendix A, we present parameter estimation results obtained under the isotropic-spin prior, which is routinely used by the LVC, and show that the posterior distributions remain bimodal.

## II. PARAMETER ESTIMATION SETUPS

We perform a suite of parameter estimation computations in order to investigate the origin of the bimodality in our posterior distributions. In all of these computations, we use the recently-developed IMRPhenomXPHM waveform model [20], which models the gravitational waves emitted by a quasi-circular precessing binary black hole. In addition to the dominant quadrupolar radiation, the model also includes higher-order multipoles in the co-precessing frame of the binary system (see below for the precise list of the available modes). This model calibrates analytic expressions of these radiation multipoles, which are accurate in the early-inspiral regime of the binary evolution, with numerical-relativity simulations that describe the merger-ringdown regime. Since the simulations have only been performed for mass ratios of  $0.25 < q < 1$  for precessing binaries [23], for smaller values of  $q$  the merger-ringdown regime as described by IMRPhenomXPHM necessarily requires an extrapolation.<sup>1</sup> For GW151226, where a large number of orbital cycles was observed in the early-inspiral stage and the inferred value of  $q \approx 0.15$  is only slightly out of the bounds, the waveform model remains a good description [20, 23]. To evaluate the evolution of the binary Euler angles due to orbital precession, we use the default angle prescription of IMRPhenomXPHM [20], which uses a hybrid of the so-called multi-scale analysis method [28] and the post-Newtonian approximation [29].

The specifications of our parameter inference setups are detailed as follows:

- **DEFAULT:** our main setup in which we include orbital precession and all of the multipole moments in IMRPhenomXPHM, which are the  $(\ell, |m|) = \{(2, 2), (2, 1), (3, 3), (3, 2), (4, 4)\}$  multipoles in the co-precessing frame [20];
- **NO HIGHER MULTIPOLES:** same as DEFAULT, except we only include the dominant  $(\ell, |m|) = (2, 2)$  multipole in the co-precessing frame of the binary. This is achieved through the multipole selection feature of the LALSuite [30] implementation of the waveform model;
- **NO PRECESSION:** same as DEFAULT, except we disable precession in the waveform model by setting the in-plane spins of the black holes to zero in the likelihood evaluation [3].<sup>2</sup>

<sup>1</sup> In fact, the need to extrapolate for binaries with  $q < 0.25$  in the merger-ringdown regime occurs for all of the current waveform models that incorporate precession and higher multipoles [20–22].

<sup>2</sup> In principle, setting the in-plane spins to zero would also nullify the effects of in-plane spin-spin interactions on the phase of the gravitational waveform [31, 32]. However, since the spin-spin interactions are neglected in the modelling of IMRPhenomXPHM [20], our proposed test is equivalent to only disabling precession.

As our choices make clear, the NO HIGHER MULTIPOLES and NO PRECESSION setups are designed to disentangle the effects of higher multipoles and orbital precession from the parameter inference of the DEFAULT setup. We shall find that only the posterior distributions of the DEFAULT setup are bimodal.

Unless stated otherwise, we adopt a prior that is uniform in the detector-frame component masses, luminosity volume, and the effective aligned spin,  $\chi_{\text{eff}} \equiv (\vec{\chi}_1 + q\vec{\chi}_2) \cdot \hat{L}/(1+q)$  [33], where  $\vec{\chi}_1$  and  $\vec{\chi}_2$  are the dimensionless component spins of the binary and  $\hat{L} \equiv \vec{L}/|\vec{L}|$  is the unit vector along the (Newtonian) orbital angular momentum. We use the flat-in- $\chi_{\text{eff}}$  prior because  $\chi_{\text{eff}}$  is the most precisely-measured spin parameter in gravitational-wave inference of binary systems. In Section IV and Appendix A, we shall discuss how our parameter estimation results would change when the isotropic-spin prior [2, 34] is instead adopted. We use relative binning [35] for fast likelihood computation, and estimate the data power spectral density (PSD) using Welch’s method, with the specifications detailed in Ref. [4]. We also include a drift correction [36] in the PSD estimation in order to account for possible evolution of the noise curve around the time of the event.

We generate the posterior samples using PyMultiNest [37–39], a nested-sampling algorithm which is capable of searching for multiple modes in the posterior distribution. Since the log likelihood of the two modes in the DEFAULT setup are distributed over vastly different volumes in parameter space, we find it necessary to choose a large number of live points [37, 38] in the sampler in order to ensure that the low- $q$  mode, which occupies a smaller volume in likelihood space, is adequately sampled. We emphasize that the volume described here is associated to the likelihood profile of the two modes, but not the volume of our choice of prior. Empirically, we find that at least 15,000 live points are needed for the DEFAULT posterior distributions to asymptotically agree with one another. Importantly, the same large number of live points is used in all of the parameter estimation setups described above, such that any absence of the low- $q$  mode reflects a genuine suppression in the likelihood of that region of parameter space, rather than due to undersampling.

### III. RESULTS

Our parameter estimation results are shown in Fig. 1, where we find that the posterior distributions of the DEFAULT setup are clearly bimodal. The bimodality can be characterized by two modes in the marginalized posterior distribution on  $q$ , with the high- $q$  and low- $q$  modes separated by a slice taken at  $q \approx 0.4$ . A summary of the median and 90% symmetric credible intervals of the inferred source parameters is provided in Table I. The high- $q$  mode, with  $q = 0.68_{-0.25}^{+0.29}$ ,  $m_1 = 12.4_{-2.1}^{+3.4} M_\odot$ ,

$m_2 = 8.4_{-1.7}^{+1.6} M_\odot$ , and  $\chi_{\text{eff}} = 0.15_{-0.07}^{+0.10}$ , is consistent with the results that have been reported in the literature [1–5]. On the other hand, the low- $q$  mode, with  $q = 0.15_{-0.06}^{+0.18}$ ,  $m_1 = 29.3_{-11.0}^{+11.4} M_\odot$ ,  $m_2 = 4.3_{-0.8}^{+1.7} M_\odot$ , and  $\chi_{\text{eff}} = 0.50_{-0.25}^{+0.14}$ , is new and qualitatively distinct. In addition to having a larger positive value of  $\chi_{\text{eff}}$  and a heavier primary source mass, the secondary source mass of the new solution could fall in the putative lower mass gap of black hole population, which is approximately at  $2.5\text{--}5M_\odot$  [25–27]. In Section IV, we shall describe how the combination of small  $q$ , large  $\chi_{\text{eff}}$ , and the presence of precession means that the spin of the primary black hole must be large. We shall also discuss how the bimodal distributions arise due to the presence of a non-trivial degeneracy between the waveforms in those two modes. Interestingly, despite the bimodality of the posterior distributions on the mass and spin parameters, the one-dimensional marginalized posteriors of the extrinsic parameters for the DEFAULT setup are unimodal. In Table I, we also report the median and 90% symmetric credible intervals of the inclination angle between the binary total angular momentum and the detector line of sight,  $\theta_{\text{JN}}$ ; the luminosity distance,  $D_L$ ; and the source redshift,  $z$ , assuming flat  $\Lambda$ CDM cosmology with the cosmological parameter values inferred by Planck [40].

From Fig. 1, we observe that the marginalized posterior probabilities of the low- $q$  mode can appear larger than those of the high- $q$  mode along some parameter directions, such as on  $q$ ,  $m_2$ , and  $\chi_{\text{eff}}$ , but smaller along others, such as on  $m_1$ . However, as we shall elaborate in Section IV and Appendix A, the relative heights of the two modes’ posterior probabilities can vary with choices of priors. For an alternative and prior-independent measure of their relative statistical significance, we plot the log likelihood distribution,  $\ln \mathcal{L}$ , of the DEFAULT setup in Fig. 1. The two-dimensional contour plots in  $\ln \mathcal{L}$  demonstrate how the low- $q$  mode has a larger log likelihood and is therefore statistically preferred by this measure. More precisely, the median and 90% symmetric credible interval of the low- $q$  and high- $q$  modes are found to be  $\ln \mathcal{L} = 91.2_{-4.5}^{+3.4}$  and  $85.5_{-4.3}^{+3.2}$ , respectively, see Table I.

The posterior distributions of the NO HIGHER MULTIPOLES and NO PRECESSION setups are also shown in Fig. 1. In these cases, the distributions are unimodal and consistent with the high- $q$  mode of the DEFAULT setup; see Table I. Crucially, the absence of the low- $q$  mode in these setups highlights the importance of *both* higher multipoles and orbital precession for the appearance of this new solution. By comparing the  $\ln \mathcal{L}$  distributions in Fig. 1, we conclude that the presence of both higher multipoles and precession in the DEFAULT low- $q$  mode is indeed statistically preferred by the data. Note that the priors used in all of these setups are identical; the absence of the low- $q$  mode in the NO HIGHER MULTIPOLES and NO PRECESSION setups therefore arises due to genuine suppression of the likelihood in that region of parameter space.

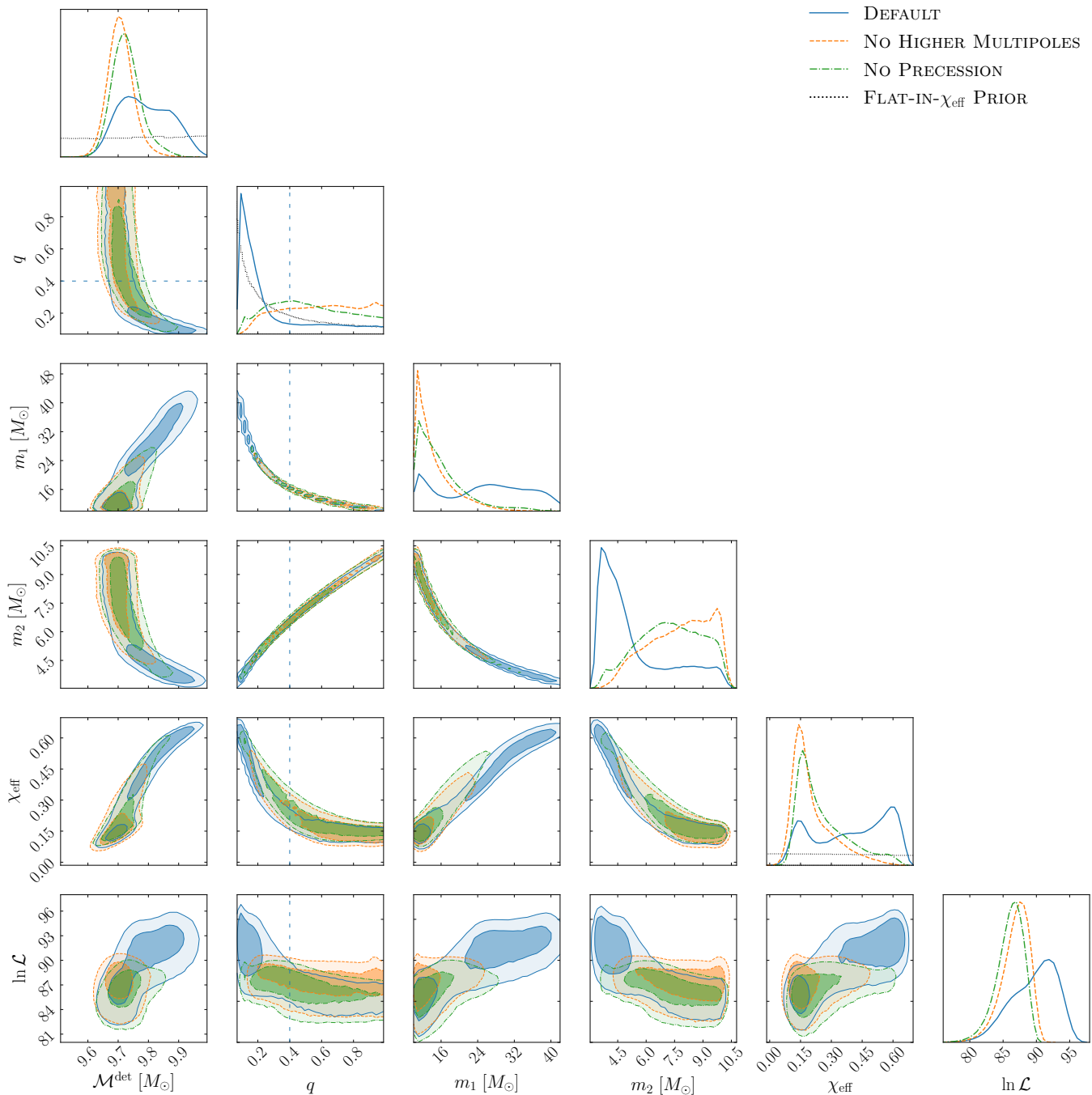


FIG. 1. Posterior distributions for GW151226 on the detector-frame chirp mass  $\mathcal{M}^{\text{det}}$ , the mass ratio  $q \equiv m_2/m_1 \leq 1$ , the primary source mass  $m_1$ , the secondary source mass  $m_2$ , the effective aligned spin  $\chi_{\text{eff}}$ , and the log likelihood,  $\ln \mathcal{L}$ . The two-dimensional contours enclose the 50% and 90% credible regions. The posterior distributions of the DEFAULT setup are clearly bimodal, while those of the NO HIGHER MULTIPOLES and NO PRECESSION setups are unimodal and consistent with the high- $q$  mode of the DEFAULT setup. The priors used in these setups are shown on the diagonal subplots, while the dashed horizontal and vertical blue lines indicate the  $q = 0.4$  slice that we choose to separate the high- $q$  and low- $q$  modes of the DEFAULT setup.

#### IV. SOURCE DISCUSSION

In the previous section, we demonstrated how the posterior distributions of the DEFAULT setup are bimodal.

Crucially, the low- $q$  mode, which has a larger average log likelihood, only emerges when both higher multipoles and orbital precession are included in the parameter inference.

	LOW- $q$ MODE	HIGH- $q$ MODE	NO HIGHER MULTIPOLES	NO PRECESSION
Detector-frame chirp mass, $\mathcal{M}^{\text{det}}$ [ $M_{\odot}$ ]	$9.82^{+0.12}_{-0.11}$	$9.70^{+0.06}_{-0.06}$	$9.71^{+0.08}_{-0.06}$	$9.72^{+0.09}_{-0.07}$
Mass ratio, $q = m_2/m_1$	$0.15^{+0.18}_{-0.06}$	$0.68^{+0.29}_{-0.25}$	$0.61^{+0.36}_{-0.40}$	$0.50^{+0.43}_{-0.34}$
Primary source mass, $m_1$ [ $M_{\odot}$ ]	$29.3^{+11.4}_{-11.0}$	$12.4^{+3.4}_{-2.1}$	$13.1^{+10.6}_{-2.8}$	$14.6^{+12.7}_{-4.1}$
Secondary source mass, $m_2$ [ $M_{\odot}$ ]	$4.3^{+1.7}_{-0.8}$	$8.4^{+1.6}_{-1.7}$	$7.9^{+2.0}_{-3.0}$	$7.3^{+2.5}_{-2.9}$
Total source mass, $M$ [ $M_{\odot}$ ]	$33.6^{+10.6}_{-9.3}$	$20.9^{+1.7}_{-0.9}$	$21.1^{+7.5}_{-1.1}$	$21.9^{+9.9}_{-1.9}$
Effective aligned spin, $\chi_{\text{eff}}$	$0.50^{+0.14}_{-0.25}$	$0.15^{+0.10}_{-0.07}$	$0.18^{+0.25}_{-0.08}$	$0.22^{+0.31}_{-0.10}$
Inclination angle, $ \cos\theta_{\text{JN}} $	$0.92^{+0.06}_{-0.12}$	$0.81^{+0.16}_{-0.30}$	$0.85^{+0.13}_{-0.30}$	$0.82^{+0.16}_{-0.35}$
Luminosity distance, $D_L$ [Mpc]	$457^{+103}_{-153}$	$464^{+150}_{-177}$	$473^{+128}_{-162}$	$471^{+157}_{-184}$
Source redshift, $z$	$0.10^{+0.02}_{-0.03}$	$0.10^{+0.03}_{-0.04}$	$0.10^{+0.02}_{-0.03}$	$0.10^{+0.03}_{-0.04}$
Log likelihood, $\ln\mathcal{L}$	$91.2^{+3.4}_{-4.5}$	$85.5^{+3.2}_{-4.3}$	$87.1^{+2.6}_{-4.2}$	$86.3^{+2.6}_{-4.1}$
Fractional sample number	76.2%	23.8%	—	—

TABLE I. Median and 90% symmetric credible interval of the source parameters and the log likelihood for the parameter estimation setups outlined in Section II. For the DEFAULT setup, we divide the bimodal posterior distributions into the low- $q$  and high- $q$  modes by slicing the samples at  $q = 0.4$  as shown in Fig. 1. In this case, the fractional number of samples in the two modes are also reported.

Why is the low- $q$  mode absent in the NO HIGHER MULTIPOLES and NO PRECESSION setups? In the former case, the absence of this mode is a manifestation of the fact that higher multipoles are more strongly excited when the binary component masses are more asymmetric [41–44]. By omitting higher multipoles in the NO HIGHER MULTIPOLES setup, we have inadvertently penalized the solutions that are most efficient at emitting these modes to begin with. Using the mode selection feature of the LALSuite implementation of IMRPhenomXPHM [20, 30], we can determine the relative

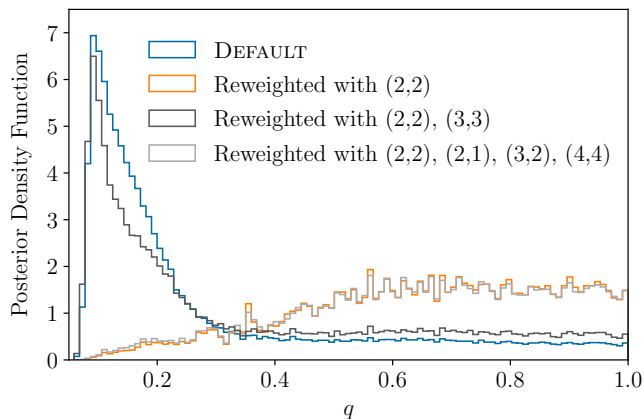


FIG. 2. Marginalized posterior distributions on  $q$  for the DEFAULT setup and for the scenarios in which the DEFAULT samples have been reweighted with other likelihoods. These likelihoods encapsulate orbital precession, the (2,2) mode in the co-precessing frame, and different subsets of higher multipoles in the co-precessing frame that are available in IMRPhenomXPHM. This figure shows that the co-precessing (3,3) mode, in addition to the dominant (2,2), is primarily responsible for the emergence of the low- $q$  mode in GW151226.

importance of the various higher multipoles in the low- $q$  mode. In particular, we achieve this by reweighting the likelihood of the DEFAULT setup with likelihoods that exclude different higher multipoles, and then compare the resulting posterior distributions [17, 18]. The results are shown in Fig. 2, where we find that the (3,3) multipole in the co-precessing frame is critical for the emergence of the low- $q$  mode. By contrast, other higher multipoles contribute marginally. Through a more refined analysis, we find that the relative importance of the multipoles in the low- $q$  mode obey the hierarchy (2,2) > (3,3) > (2,1) > (4,4) > (3,2). We note that Ref. [16] had also analyzed the importance of higher multipoles in GW151226 through the likelihood reweighting method described here [17, 18], though since precession was omitted in that work the analysis effectively only applied to the high- $q$  mode.

The absence of the low- $q$  mode in the NO PRECESSION setup implies that the primary black hole has a large in-plane spin component. This can be understood from the fact that orbital precession, which is governed by the following equation at leading order [14, 31, 32]

$$\frac{d\vec{L}}{dt} = \frac{m_1^2}{r^3} \left[ \left( 2 + \frac{3q}{2} \right) \vec{\chi}_1 + \left( 2q^2 + \frac{3q}{2} \right) \vec{\chi}_2 \right] \times \vec{L}. \quad (1)$$

is mainly driven by the in-plane spin of the heavier black hole when  $q$  is small. In Fig. 3, we plot the posterior distributions of the heavier black hole’s in-plane spin for our various parameter estimation setups. The lighter black hole’s spin is unconstrained and therefore not shown in this work. We found empirically that the two-dimensional posterior distributions on the in-plane spin components,  $\chi_{1x}$  and  $\chi_{1y}$ , exhibited two similar modes that are related through a rotation of  $180^\circ$  on this plane. This is the case because the orientation of

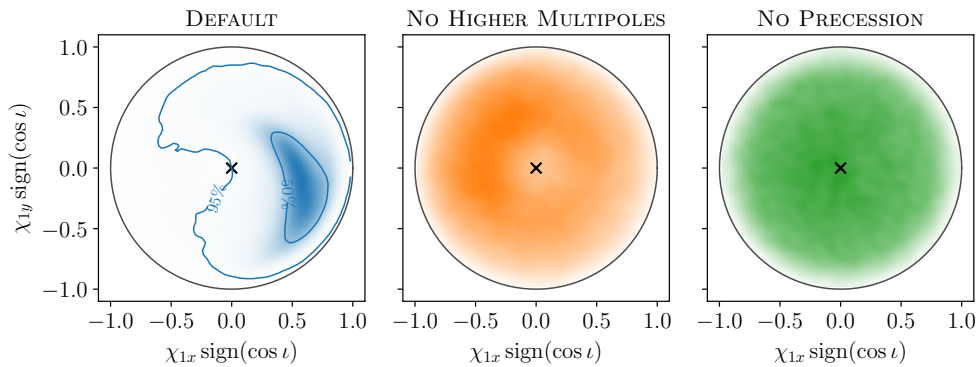


FIG. 3. Posterior distributions on the in-plane spin components of our various parameter estimation setups. We multiply a factor of  $\text{sign}(\cos \iota)$  on each of the spin components because the figures, especially the left panel, would otherwise display two modes that are similar up to a  $180^\circ$  rotation in the azimuthal direction, due to the reflection degeneracy in the measured orientation of the orbit. For the DEFAULT setup, we show the 50% and 95% credible regions, and find that zero in-plane spin (black cross) is excluded at the 95% credible level. Due to precessional motion, the position of the DEFAULT in-plane spin evolves in the azimuthal direction; in this work, we use the reference frequency  $f_{\text{ref}} = 100$  Hz (see main text for motivation). Recall that the NO PRECESSION setup is designed such that the in-plane spins are ignored in the likelihood evaluation – the distribution in the right panel therefore corresponds to our prior used for these variables.

the orbit is only determined up to a reflection degeneracy about the orbital plane. For this reason, in Fig. 3 we show the posteriors on  $\chi_{1x} \text{sign}(\cos \iota)$  and  $\chi_{1y} \text{sign}(\cos \iota)$  which collapses the two modes into a single mode, where  $\iota$  is the inclination angle between the binary orbital angular momentum and the detector line of sight. Note that the definitions of  $\chi_{1x}, \chi_{1y}$  and  $\iota$  depend on the reference frequency,  $f_{\text{ref}}$ , at which the source is specified, as these parameters evolve with time due to precessional motion. In this work, we choose  $f_{\text{ref}} = 100$  Hz, which is close to the detectors’ peak sensitivities, because the spin variables are better measured at this frequency compared to lower frequencies [45] and for more efficient parameter estimation calculation [46].

From Fig. 3, we find that the primary black hole of the DEFAULT setup has a large in-plane spin, which excludes zero at the 95% credible level. Although not shown explicitly in this figure, this non-zero spin is dominated by the posterior samples in the low- $q$  mode. For the NO PRECESSION setup, we observe that the posterior distribution is distributed approximately uniformly on the  $(\chi_{1x} \text{sign}(\cos \iota), \chi_{1y} \text{sign}(\cos \iota))$  plane. This is the case because the in-plane spins do not contribute to the likelihood evaluation of this setup, see Section II, and are thus orthogonal to the parameter estimation process. The observed distribution for the NO PRECESSION setup is therefore exactly the spin components that are sampled by PyMultiNest from the prior, which we have taken to be uniformly distributed in  $\cos \iota$  and in the  $\chi_{1x}^2 + \chi_{1y}^2 = 1 - \chi_{1z}^2$  disk, with  $\chi_{1z}$  being the spin component along the orbital angular momentum. Since the posterior distribution of the NO HIGHER MULTIPOLES setup in Fig. 3 is almost uniformly distributed, we conclude that precession is not well measured in this setup.

Motivated by the mass-weighted spin combination in

(1), the effective precession parameter [14]

$$\chi_p \equiv \max \left( |\vec{\chi}_1 \times \hat{L}|, \frac{4q^2 + 3q}{4 + 3q} |\vec{\chi}_2 \times \hat{L}| \right), \quad (2)$$

is often used as a measure for precession. In Fig. 4, we plot the posterior distributions on  $\chi_p$  for our various parameter estimation setups. Recall that the  $\chi_p$  distribution of the NO PRECESSION setup represents the case in which orbital precession is intentionally disabled in the waveform during likelihood evaluation, see Section II; it therefore serves as a useful null comparison for tests of precession in other scenarios [3]. For instance, since the  $\chi_p$  distribution of the NO HIGHER MULTIPOLES setup is very similar to that of the NO PRECESSION setup, we

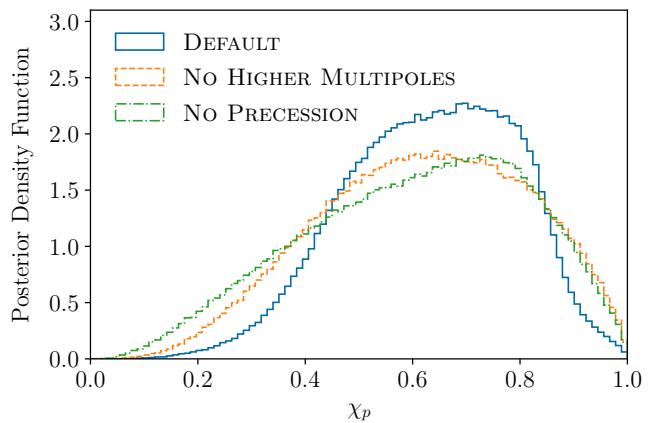


FIG. 4. Marginalized posterior distributions on  $\chi_p$  for our various parameter estimation setups. The distribution of the NO PRECESSION setup represents the case in which orbital precession is intentionally disabled in the likelihood evaluation, and therefore serves as a useful null comparison for tests of precession in other scenarios.

conclude that precession is not well measured in this scenario – a conclusion that is in agreement with Fig. 3. On the other hand, the  $\chi_p$  distribution of the DEFAULT setup manifestly deviates away from the NO PRECESSION case, indicating that this setup displays signs of precession. Having said that, unlike Fig 3, it is difficult to infer the degree to which orbital precession is important in the DEFAULT setup from Fig. 4.<sup>3</sup>

In addition to having a non-negligible primary in-plane spin, the low- $q$  mode of the DEFAULT setup also has a modestly large value of  $\chi_{\text{eff}}$ , see Fig. 1 and Table I. This is especially interesting because  $\chi_{\text{eff}}$  in the small- $q$  limit is also dominated by the spin of the primary black hole, albeit along the direction of the orbital angular momentum. The primary spin of this mode is therefore not only tilted away from both the orbital angular momentum and the orbital plane, but must also have a large magnitude. In Fig. 5, we show the contour plots of the DEFAULT setup on  $\chi_{\text{eff}}$ , the primary spin magnitude,  $|\vec{\chi}_1|$ , and the inclination angle between the primary spin and the orbital angular momentum,  $\theta_{1L}$ , at  $f_{\text{ref}} = 100$  Hz. From the  $(\chi_{\text{eff}}, |\vec{\chi}_1|)$  contour, we find that the primary black hole indeed spins very rapidly – in fact close to extremality – with  $|\vec{\chi}_1| = 0.88^{+0.11}_{-0.14}$ . The tilt of the primary spin  $\theta_{1L} = (47^{+15}_{-18})^\circ$  is less well-constrained, although it still provides  $\gtrsim 90\%$  confidence that the primary spin neither aligns with the orbital angular momentum nor lies in the orbital plane.

In order to ensure that our primary spin measurement is robust against changes to spin priors, we repeat the parameter estimation calculation for the DEFAULT setup but with a prior that is uniform in spin magnitude and isotropic in spin orientation for each of the black hole (the priors on other parameters are unchanged). This so-called isotropic-spin prior is routinely used in the parameter inferences conducted by the LVC [2, 34] and, unlike the flat-in- $\chi_{\text{eff}}$  prior, is suppressed at large values of  $|\chi_{\text{eff}}|$ , see Fig. 5 and e.g. Ref. [47]. The posterior distributions of this new setup are also shown in Fig. 5, which we distinguish from the previous case by explicitly labeling their prior names. The posterior distributions with this new prior on other source parameters are relegated to Fig. 8 in Appendix A. From Fig. 5, we see that the probability of the high- $\chi_{\text{eff}}$  mode, equivalently

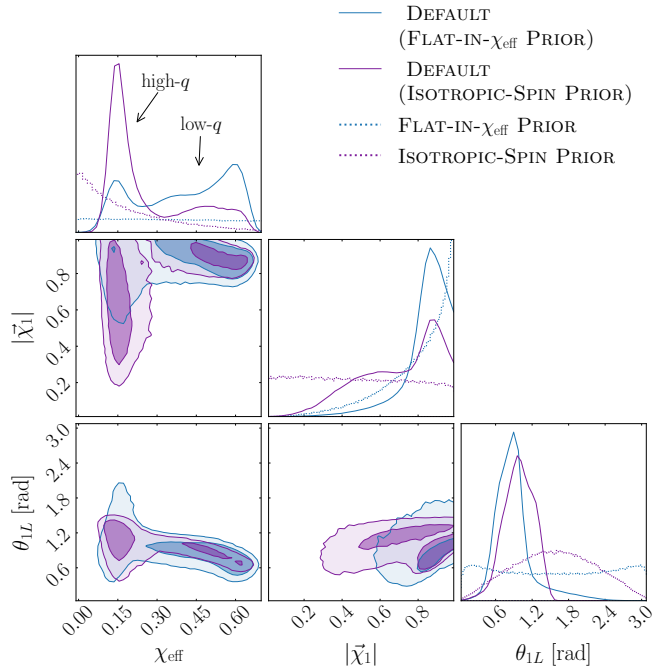


FIG. 5. Posterior distributions on  $\chi_{\text{eff}}$ , the primary spin magnitude,  $|\vec{\chi}_1|$ , and the inclination angle between the primary spin and the orbital angular momentum,  $\theta_{1L}$ , at the reference frequency  $f_{\text{ref}} = 100$  Hz. Here we show the DEFAULT posterior distributions evaluated with the flat-in- $\chi_{\text{eff}}$  prior and the isotropic-spin prior, both of which are also in the diagonal subplots. Recall from Fig. 1 that the high- $\chi_{\text{eff}}$  and low- $\chi_{\text{eff}}$  modes are synonymous to the low- $q$  and high- $q$  modes, respectively.

the low- $q$  mode, is partially suppressed in the isotropic-spin prior case with respect to the flat-in- $\chi_{\text{eff}}$  prior case, due to the prior volume suppression mentioned above. Crucially, from the  $(\chi_{\text{eff}}, |\vec{\chi}_1|)$  plot, we conclude that the contour region of  $|\vec{\chi}_1|$  for the low- $q$  mode remains largely unchanged between the two setups. This corroborates our finding above that the primary black hole in the low- $q$  mode spins very rapidly. By contrast, the  $|\vec{\chi}_1|$  posterior of the low- $\chi_{\text{eff}}$  mode, equivalently the high- $q$  mode, becomes manifestly broader and is thus not well-constrained. The spin of the secondary black hole is also virtually unconstrained by the data and is therefore not shown in this paper.

Finally, we note that multimodal posterior distributions are rarely observed in the source parameters of gravitational-wave sources. A notable exception is the analysis conducted in Refs. [48, 49], which found that the posterior distributions of GW190521 [50] exhibit multimodal behaviors under different choices of mass priors. The rareness of multi modality makes GW151226 an especially interesting event, as it provides a concrete example in which waveforms in fairly different regions of parameter space can be nearly degenerate with one another. In Fig. 6, we plot the whitened waveforms of the maximum likelihood solutions in the low- $q$  and high- $q$

<sup>3</sup> As noted in Ref. [3], the precise value and shape of any  $\chi_p$  distribution should not be overly interpreted, as they depend on the measured values of  $q$  and  $\chi_{\text{eff}}$  as well. For instance, although the NO PRECESSION setup contains no information about precession, its  $\chi_p$  posterior distribution in Fig. 4 broadly peaks around  $\chi_p \sim 0.8$ , instead of  $\chi_p \sim 0$ , because the Kerr bound  $|\vec{\chi}_1| \leq 1$  and  $|\vec{\chi}_2| \leq 1$  correlates  $\chi_p$  with the other spin components, with the latter additionally constrained by the data [2, 3]. Similarly, the DEFAULT setup is inferred to display signs of precession in Fig. 4 not because of the precise shape of its  $\chi_p$  distribution, but because of its difference with the  $\chi_p$  distribution of the NO PRECESSION setup.

modes, for both the LIGO Hanford and Livingston detector strain data. By visual inspection, we see that these maximum likelihood waveforms indeed look very similar to each other. For a more quantitative measure of the degree of degeneracy between the waveforms in the low- $q$  and high- $q$  modes, we randomly draw 5,000 samples from each mode and compute their overlaps with the maximum likelihood waveform, which falls in the low- $q$  mode. The overlap is defined through the inner product [51]

$$(h_i|h_j) = 4 \operatorname{Re} \int_{f_{\text{lo}}}^{f_{\text{hi}}} df \frac{\tilde{h}_i^*(f) \tilde{h}_j(f)}{S_n(f)}, \quad (3)$$

where  $h_{i,j}$  are two arbitrary waveforms,  $\tilde{h}_{i,j}$  are their Fourier representations, asterisk denotes complex conjugation,  $S_n$  is the noise power spectral density, and  $f_{\text{lo}} = 20$  Hz and  $f_{\text{hi}} = 512$  Hz are the lower and upper cutoff frequencies that we adopt for the integral, respectively. In Fig. 7, we show the normalized overlaps,  $(h_i|h_j)/[(h_i|h_i)(h_j|h_j)]^{1/2}$ , between those random samples and the maximum likelihood waveform using the Hanford detector's noise curve (the equivalent plot for the Livingston detector looks similar to Fig. 7 and is not shown in this paper). We find that most of the overlaps are distributed within 0.92–0.99, which are indeed highly non-trivial values. While the cause of this degeneracy remains unclear, we speculate that it traces its origin to the well-known degeneracy between  $q$  and  $\chi_{\text{eff}}$  in the phase of binary waveforms [51–53], which seem to be present in the  $(q, \chi_{\text{eff}})$  contour of the DEFAULT samples in Fig. 1.

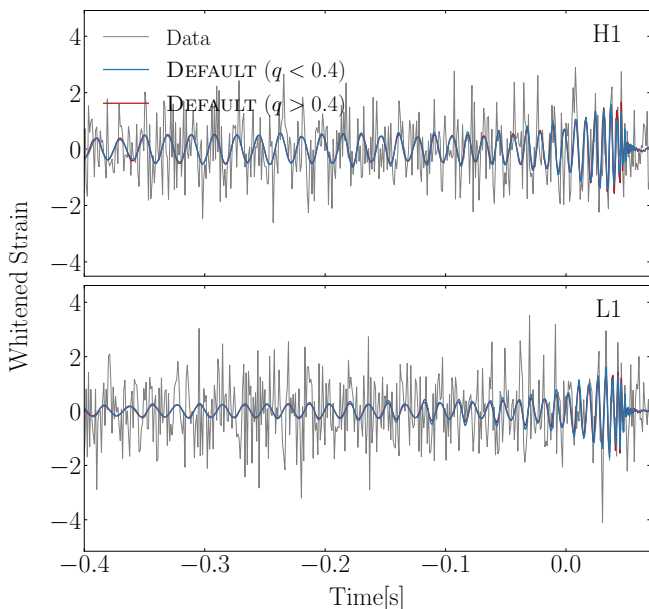


FIG. 6. Whitenened data of the LIGO Hanford (top panel) and Livingston (bottom panel) detectors near the merger time of GW151226. In each of these panels, we also show the whitened waveforms of the maximum likelihood solution in the low- $q$  and high- $q$  modes.

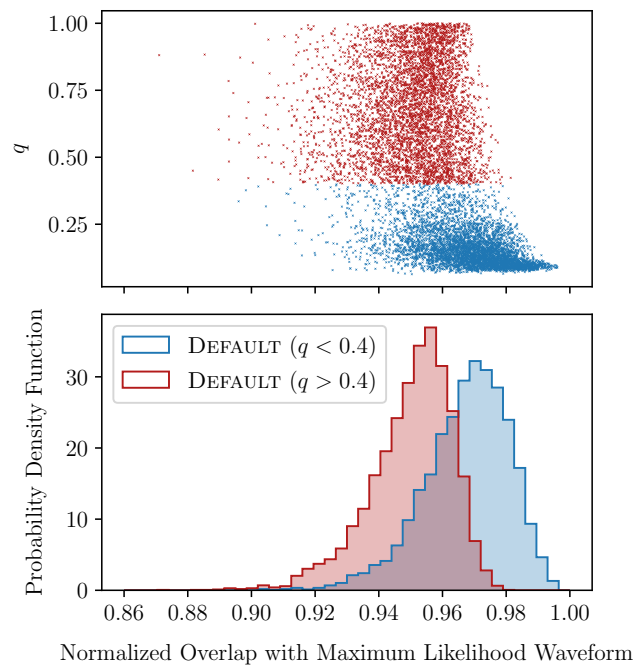


FIG. 7. Distributions of the normalized overlap between random waveform samples in the two modes and the maximum likelihood waveform, which lies in the low- $q$  mode. Here we only show the distributions computed with the LIGO Hanford data; the equivalent plot for LIGO Livingston looks similar and is omitted in this paper.

We hope to further investigate the origin of this degeneracy in future work.

## V. ASTROPHYSICAL IMPLICATIONS

Because the source properties of the low- $q$  mode are different from those of the high- $q$  mode, the true astrophysical interpretation of GW151226 could be different from what was inferred in the literature. In fact, the combination of small  $q$ , large  $\chi_{\text{eff}}$ , and non-vanishing precession makes the low- $q$  mode of GW151226 an outlier in the known population of merging black holes, as most of the signals detected to date have comparable component masses, small values of  $\chi_{\text{eff}}$ , and display no signs of precession [2–5, 24, 34]. In the following, we assume that GW151226 is entirely described by the low- $q$  mode and briefly explore its astrophysical implications.

Asymmetric-mass binary systems are relatively uncommon in the observed population of binary black holes [2, 3, 5, 34]. In this respect, the low- $q$  mode of GW151226 is similar to GW190412 [54] and GW190814 [55], whose mass ratios of  $q = 0.28_{-0.06}^{+0.12}$  and  $q = 0.112_{-0.009}^{+0.008}$  make them the two most asymmetric binary systems observed by the LVC to date. The two broad classes of formation channels for merging black holes, which are the canonical isolated binary evolution channel [56–59] and the dynamical merger chan-



nel [60–66], typically predict orders of magnitude more comparable-mass binary black holes than asymmetric-mass binary systems [67–72]. A measurement of  $q$  alone therefore does not immediately inform us about the formation history of GW151226, though it is interesting that GW151226 increases the sample size of asymmetric-mass binary systems, which could provide better statistical constraints on the formation channels mentioned above, including constraints on their branching fractions.

The secondary mass  $m_2 = 4.3_{-0.8}^{+1.7} M_\odot$  of the low- $q$  mode could lie in the hypothesized lower mass gap of  $2.5\text{--}5 M_\odot$  [25–27]. The lower bound of the mass gap is determined by the maximum mass of neutron stars, with the uncertainties governed by the stars’ modestly constrained nuclear equation of state [73–75]. On the other hand, the upper bound is empirically inferred from observations of X-ray binaries [25–27] and theoretically depend on the details of the explosion and implosion mechanisms of stellar cores [76, 77]. Assuming that the upper bound is located precisely at  $5 M_\odot$ , the probability that the low- $q$  mode falls in the mass gap is 60% if we use the full bimodal DEFAULT posterior, or 79% if we restrict ourselves to the  $q < 0.4$  samples. Most of the binary black holes observed to date, except GW190814,<sup>4</sup> have component masses that are above this gap; GW151226 therefore offers a tantalizing hint for the presence of such a mass-gap black hole, though future observations are certainly needed in order to confidently address this puzzle.

Spin measurements offer valuable probes into the formation mechanisms of merging black holes [81, 82]. As illustrated in Fig. 5, the primary spin of the low- $q$  mode is not only tilted away from the orbital angular momentum, but also has a large magnitude  $|\vec{\chi}_1| = 0.88_{-0.14}^{+0.11}$ . On the other hand, the secondary spin is virtually unconstrained. If GW151226 was formed through the canonical isolated binary evolution channel [56–59], the spin measurement in Fig. 5 suggests that some of the first-born black holes in this formation channel can attain large natal spins. Nevertheless, a highly-spinning primary black hole seems unlikely theoretically because angular momentum transport from the progenitor star’s helium core to the hydrogen envelope is typically very efficient during the red supergiant phase, resulting in a remnant core that has little angular momentum before it collapses to a black hole [83–85]. Tidal interactions could in principle spin up the helium core, although this would be very inefficient before the common envelope phase [56–59], as the binary separation would still be large. Having said that, if the binary progenitor stars were born in tight orbits, they could acquire large spins through their strong tidal interactions, leading to substantial chemical mixing in both stars [86, 87]. This mixing prevents significant

expansions of stars, thereby further suppressing angular momentum loss through stellar winds or accretion. Because the spins of field binaries are preferentially aligned with the orbital angular momentum, the observed misalignment between  $\vec{\chi}_1$  and  $\vec{L}$  would most likely arise from a natal kick which is imparted by the non-spherical core collapse supernova of the progenitor stars [7, 88, 89]. For the chemically-homogeneous evolution channel, the spin misalignment angle is typically small because the orbital velocity is large (due to the small binary separation) compared to the kick velocity [86]. While this expectation may seem to contradict with our  $\theta_{1L} = (47_{-18}^{+15})^\circ$  finding, that picture largely applies to comparable-mass binary systems  $q \gtrsim 0.3$  [86] and could change for binary systems with small mass ratios.

The measured spin parameters of the low- $q$  mode can alternatively be explained if GW151226 was formed through the dynamical capture of black holes in dense stellar environments [60–66]. In this scenario, the black hole spins are expected to be randomly and isotropically distributed, which would naturally explain the measured misalignment between  $\vec{\chi}_1$  and  $\vec{L}$ . While the distributions of black hole spin magnitudes in dense stellar environments are highly uncertain, in the hierarchical merger scenario [90–92], mergers of first-generation black holes would form second- or higher-generation black holes with spins that are distributed approximately around  $|\vec{\chi}| \approx 0.7$  [93–95], as a result of converting the pre-merger orbital angular momentum to the final black hole’s spin. The precise value of the final spin depends on the mass ratio and the spin configurations of the previous-generation black holes [96–98]. If the primary black hole of GW151226 is a remnant of a first-generation merger, the large spin magnitude  $|\vec{\chi}_1| = 0.88_{-0.14}^{+0.11}$  of the low- $q$  mode could be achieved provided the spins of the first-generation black holes are modestly large and approximately oriented along the direction of the orbital angular momentum [96–98]. This spin configuration typically gives rise to a large merger kick, with only a small fraction of the second-generation black holes expected to be retained in dense stellar environments [92]. Having said that, this small fraction is consistent with the fact that GW151226 is a rare event among the observed population of merging binary black holes [2–5, 24, 34].

We can use the LVC data to estimate how likely it was for GW151226 to form through the hierarchical merger scenario, with the primary black hole being a second-generation black hole and the secondary black hole being a counterpart from any generation. From the GWTC-1 and GWTC-2 catalogs [2, 34], we find that there are about ten binary black holes whose total masses are distributed within the 90% confidence interval of  $29.3_{-11.0}^{+11.4} M_\odot$ , which is the measured primary mass of the low- $q$  mode (we neglect mass loss due to gravitational-wave radiation for simplicity). Assuming that all of those ten binaries were first-generation black hole coalescences in dense clusters, the observed ratio of first-

<sup>4</sup> Although the secondary mass of GW190814 was found to be  $2.59 M_\odot$  [55], it remains unclear if it is a heavy neutron star or a light black hole [55, 78–80].

generation mergers to a GW151226-like merger would be about 10 : 2, where we consider GW190412 to be similar to GW151226 because its mass ratio is also small and its primary spin could be large [55].<sup>5</sup> This estimation translates to a  $\sim 20\%$  capture efficiency between the second- and other-generation black holes within this mass range. Since those ten binary black holes have  $q \gtrsim 0.5$  and their chirp masses are distributed randomly around that of GW151226, the average volume up to which one can observe GW151226 is smaller than those of the first-generation mergers by a factor of about 1–1.5, due to the smaller  $q \approx 0.15$  of GW151226 [99, 100]. Correcting for this observational bias would increase the estimation above, though not by a significant amount. Our naive  $\sim 20\%$  estimate appears to be larger or roughly of the same order of magnitude as the capture efficiencies expected from population synthesis models in dense stellar systems, though the detailed predictions depend sensitively on the initial conditions assumed for the black hole and stellar populations in these dense environments [92, 101]. This naive comparison suggests that GW151226 could be formed through hierarchical mergers, though we note that the estimate above would rapidly increase if we relax the optimistic assumption that all of the ten binaries were first-generation black hole mergers in dense clusters. This would also suggest that GW151226 is only consistent with having formed through hierarchical mergers if a sizeable fraction of detectable events arise from dense stellar clusters. Recent analyses [24, 102] of the O1–O3a binary black hole population suggest that this fraction is indeed sizable, though its value is not very precisely constrained. It would be interesting to see if our estimation above would change when more data is collected in the future.

## VI. CONCLUSION

In this paper, we inferred the source parameters of GW151226 with IMRPhenomXPHM [20], a model which incorporates higher multipoles and orbital precession in the gravitational waveform of a quasi-circular binary black hole. As shown in Fig. 1, the posterior distributions of the source parameters for GW151226 are bimodal when both higher multipoles and orbital precession are included in the parameter inference – a behaviour that is clearly absent when either one of these physical effects is omitted. The bimodality can be characterized by two modes that are separated in mass ratio: a high- $q$  mode, which is consistent with the results reported in the literature [1–5], and a low- $q$  mode, which is new and has

distinct source properties. Although the relative posterior probability of these two modes can vary depending on choices of priors, as shown in Figs. 5 and 8, the low- $q$  mode has a median log likelihood that is about six points larger than that of the high- $q$  mode and is therefore statistically more significant by this measure.

The emergence of the low- $q$  mode raises the intriguing possibility that GW151226 is an entirely different type binary system from what was previously inferred in the literature. The low- $q$  mode is interesting especially because it possesses source properties that are considered rare among the observed population of merging black holes [24, 34]: its mass ratio is small, its secondary mass could fall in the lower mass gap, its primary spin magnitude is large, and its primary spin component along the orbital plane is sufficiently large to drive orbital precession. It would be interesting to see if similar types of binary signals are detected in the future, and if so how they would shed light on the astrophysical formation mechanisms of merging binary black holes.

A key takeaway of this work is that the exclusion of physical effects that are relevant to a binary system can have significant impacts on its parameter estimation. Although previous works have studied the improvements in parameter estimation that one can achieve when more physical effects are included in waveform models, see e.g. Refs. [103–105], those works only saw overall changes in the positions and shapes of unimodal posterior distributions. Here, we find that the situation could be more dramatic, in that an entirely plausible solution with a higher likelihood could emerge (see also Refs. [48, 49]). We note, however, that the inferred  $q \approx 0.15$  for the low- $q$  mode is strictly beyond the  $0.25 < q < 1$  range simulated for binary black holes in the merger regime in numerical relativity [23], though these numeric waveforms seem to work well even when extrapolated towards  $q = 1/6 \approx 0.16$  [20, 23] (see also Footnote 1). In any case, GW151226 was observed over many orbital cycles in the inspiral regime, in which analytic expressions for the waveforms remain reliable for  $q \approx 0.15$  [20, 41]. Having said that, it will be interesting to see if future improvements in waveform modeling would significantly alter the conclusions drawn in this paper. In future work, we hope to further investigate the origin of the degeneracy between the high- $q$  and low- $q$  modes in GW151226, which was illustrated in Figs. 6 and 7, and explore the general conditions under which such bimodality would appear in gravitational-wave parameter inferences. All in all, this work demonstrates the importance of detailed waveform modeling for accurate parameter estimation, and motivates further advancements in the waveform modeling frontier.

<sup>5</sup> Although GW190814 has a small mass ratio, it is different from GW151226 and GW190412 because its measured primary spin  $|\bar{\chi}_1| \leq 0.07$  is tightly constrained away from the expected value for a remnant black hole,  $|\bar{\chi}_1| \approx 0.7$  [34], and is therefore inconsistent with being a second-generation black hole.

## ACKNOWLEDGEMENTS

HSC gratefully acknowledges support from the Rubicon Fellowship awarded by the Netherlands Organisation for Scientific Research (NWO). SO acknowledges support from the National Science Foundation Graduate Research Fellowship Program under Grant No. DGE-2039656. Any opinions, findings, and conclusions or recommendations expressed in this material are those of the authors and do not necessarily reflect the views of the National Science Foundation. LD acknowledges support from the Michael M. Garland startup research grant at the University of California, Berkeley. TV acknowledges support by the National Science Foundation under Grant No. 2012086. BZ is supported by a research grant from the Ruth and Herman Albert Scholarship Program for New Scientists. MZ is supported by NSF grants PHY-1820775 the Canadian Institute for Advanced Research (CIFAR) Program on Gravity and the Extreme Universe and the Simons Foundation Modern Inflationary Cosmology initiative.

This research has made use of data, software and/or web tools obtained from the Gravitational Wave Open Science Center (<https://www.gw-openscience.org/>), a service of LIGO Laboratory, the LIGO Scientific Collaboration and the Virgo Collaboration. LIGO Laboratory and Advanced LIGO are funded by the United States National Science Foundation (NSF) as well as the Science and Technology Facilities Council (STFC) of the United Kingdom, the Max-Planck-Society (MPS), and the State of Niedersachsen/Germany for support of the construction of Advanced LIGO and construction and operation of the GEO600 detector. Additional support for Advanced LIGO was provided by the Australian Research Council. Virgo is funded, through the European Gravitational Observatory (EGO), by the French Centre National de Recherche Scientifique (CNRS), the Italian Istituto Nazionale di Fisica Nucleare (INFN) and the Dutch Nikhef, with contributions by institutions from Belgium, Germany, Greece, Hungary, Ireland, Japan, Monaco, Poland, Portugal, Spain.

### Appendix A: DEFAULT Parameter Estimation with the Isotropic-Spin Prior

In this appendix, we show the parameter estimation results for the DEFAULT setup evaluated with the isotropic-spin prior. As described in Section IV, the isotropic-spin prior consists of a distribution that is uniform in spin magnitude and isotropic in spin orientation for each of the black hole. This prior is routinely used by the LVC in their parameter estimation studies [2, 34], and is astrophysically motivated if the binary system is formed through dynamical capture. In what follows, we differentiate the DEFAULT setups evaluated with the flat-in- $\chi_{\text{eff}}$  prior and isotropic-spin prior with the nomen-

clatures DEFAULT (FLAT-IN- $\chi_{\text{eff}}$  PRIOR) and DEFAULT (ISOTROPIC-SPIN PRIOR).

The results for the DEFAULT (ISOTROPIC-SPIN PRIOR) setup are shown in Fig. 5, where we find that the posterior distributions remain bimodal. For ease of comparison, we duplicate the results of the DEFAULT (FLAT-IN- $\chi_{\text{eff}}$  PRIOR), which was shown in Fig. 1, in this figure. Since the prior volume of the isotropic-spin prior is suppressed at large values of  $|\chi_{\text{eff}}|$ , the posterior probability of the low- $q$  mode in the isotropic-spin case is relatively diminished. Having said that, unlike the NO HIGHER MULTIPOLES and NO PRECESSION cases, the low- $q$  mode is clearly present in the DEFAULT setup regardless of choices of priors. Crucially, the low- $q$  mode has a larger log likelihood than the high- $q$  mode in both DEFAULT setups, and therefore plays an important role in the astrophysical interpretation of GW151226.

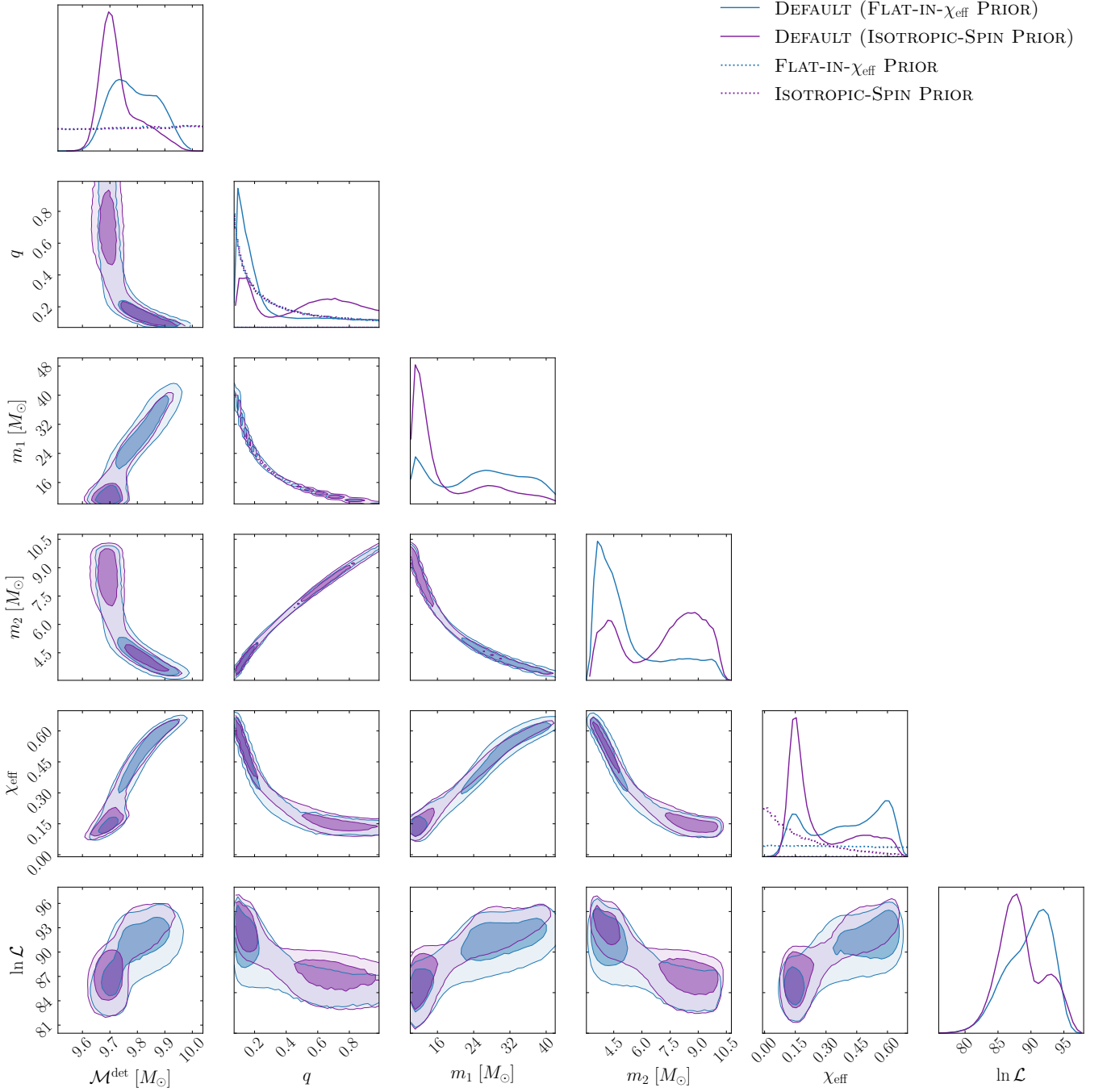


FIG. 8. Same as Fig. 1, except we show the posterior distributions of the DEFAULT setups evaluated with the flat-in- $\chi_{\text{eff}}$  prior and the isotropic-spin prior. The posterior distributions in both of these cases are clearly bimodal, though in the isotropic-spin case the posterior probability of the low- $q$  mode is relatively diminished due to the prior volume suppression at large values of  $|\chi_{\text{eff}}|$ . The two priors are identical other than for the spin variables, see also Fig. 5.

- [1] B. P. Abbott *et al.* (LIGO Scientific, Virgo), *Phys. Rev. Lett.* **116**, 241103 (2016), arXiv:1606.04855 [gr-qc].
- [2] B. P. Abbott *et al.* (LIGO Scientific, Virgo), *Phys. Rev. X* **9**, 031040 (2019), arXiv:1811.12907 [astro-ph.HE].
- [3] B. Zackay, T. Venumadhav, L. Dai, J. Roulet, and M. Zaldarriaga, *Phys. Rev. D* **100**, 023007 (2019), arXiv:1902.10331 [astro-ph.HE].
- [4] T. Venumadhav, B. Zackay, J. Roulet, L. Dai, and M. Zaldarriaga, *Phys. Rev. D* **100**, 023011 (2019), arXiv:1902.10341 [astro-ph.IM].
- [5] A. H. Nitz, T. Dent, G. S. Davies, S. Kumar, C. D. Capano, I. Harry, S. Mozzon, L. Nuttall, A. Lundgren, and M. Tápai, *Astrophys. J.* **891**, 123 (2020), arXiv:1910.05331 [astro-ph.HE].
- [6] S. Chatterjee, C. L. Rodriguez, V. Kalogera, and F. A. Rasio, *Astrophys. J. Lett.* **836**, L26 (2017), arXiv:1609.06689 [astro-ph.GA].
- [7] R. O’Shaughnessy, D. Gerosa, and D. Wysocki, *Phys. Rev. Lett.* **119**, 011101 (2017), arXiv:1704.03879 [astro-ph.HE].
- [8] N. Yunes, K. Yagi, and F. Pretorius, *Phys. Rev. D* **94**, 084002 (2016), arXiv:1603.08955 [gr-qc].
- [9] B. P. Abbott *et al.* (LIGO Scientific, Virgo), *Phys. Rev. D* **100**, 104036 (2019), arXiv:1903.04467 [gr-qc].
- [10] M. Pürrer, *Phys. Rev. D* **93**, 064041 (2016), arXiv:1512.02248 [gr-qc].
- [11] S. Khan, S. Husa, M. Hannam, F. Ohme, M. Pürrer, X. Jiménez Forteza, and A. Bohé, *Phys. Rev. D* **93**, 044007 (2016), arXiv:1508.07253 [gr-qc].
- [12] A. Taracchini *et al.*, *Phys. Rev. D* **89**, 061502 (2014), arXiv:1311.2544 [gr-qc].
- [13] M. Hannam, P. Schmidt, A. Bohé, L. Haegel, S. Husa, F. Ohme, G. Pratten, and M. Pürrer, *Phys. Rev. Lett.* **113**, 151101 (2014), arXiv:1308.3271 [gr-qc].
- [14] P. Schmidt, F. Ohme, and M. Hannam, *Phys. Rev. D* **91**, 024043 (2015), arXiv:1408.1810 [gr-qc].
- [15] Y. Pan, A. Buonanno, A. Taracchini, L. E. Kidder, A. H. Mroué, H. P. Pfeiffer, M. A. Scheel, and B. Szilágyi, *Phys. Rev. D* **89**, 084006 (2014), arXiv:1307.6232 [gr-qc].
- [16] E. Payne, C. Talbot, and E. Thrane, *Phys. Rev. D* **100**, 123017 (2019), arXiv:1905.05477 [astro-ph.IM].
- [17] C. P. Robert and G. Casella, *Monte Carlo Statistical Methods (Springer Texts in Statistics)* (Springer-Verlag, Berlin, Heidelberg, 2005).
- [18] J. S. Liu, *Monte Carlo Strategies in Scientific Computing* (Springer Publishing Company, Incorporated, 2008).
- [19] V. Varma, S. E. Field, M. A. Scheel, J. Blackman, L. E. Kidder, and H. P. Pfeiffer, *Phys. Rev. D* **99**, 064045 (2019), arXiv:1812.07865 [gr-qc].
- [20] G. Pratten *et al.*, (2020), arXiv:2004.06503 [gr-qc].
- [21] S. Khan, F. Ohme, K. Chatzioannou, and M. Hannam, *Phys. Rev. D* **101**, 024056 (2020), arXiv:1911.06050 [gr-qc].
- [22] S. Ossokine *et al.*, *Phys. Rev. D* **102**, 044055 (2020), arXiv:2004.09442 [gr-qc].
- [23] V. Varma, S. E. Field, M. A. Scheel, J. Blackman, D. Gerosa, L. C. Stein, L. E. Kidder, and H. P. Pfeiffer, *Phys. Rev. Research*. **1**, 033015 (2019), arXiv:1905.09300 [gr-qc].
- [24] R. Abbott *et al.* (LIGO Scientific, Virgo), (2020), arXiv:2010.14533 [astro-ph.HE].
- [25] C. D. Bailyn, R. K. Jain, P. Coppi, and J. A. Orosz, *Astrophys. J.* **499**, 367 (1998), arXiv:astro-ph/9708032.
- [26] F. Ozel, D. Psaltis, R. Narayan, and J. E. McClintock, *Astrophys. J.* **725**, 1918 (2010), arXiv:1006.2834 [astro-ph.GA].
- [27] W. M. Farr, N. Sravan, A. Cantrell, L. Kreidberg, C. D. Bailyn, I. Mandel, and V. Kalogera, *Astrophys. J.* **741**, 103 (2011), arXiv:1011.1459 [astro-ph.GA].
- [28] K. Chatzioannou, A. Klein, N. Yunes, and N. Cornish, *Phys. Rev. D* **95**, 104004 (2017), arXiv:1703.03967 [gr-qc].
- [29] S. Marsat, L. Blanchet, A. Bohe, and G. Faye (2013) arXiv:1312.5375 [gr-qc].
- [30] LIGO Scientific Collaboration, “LIGO Algorithm Library - LALSuite,” free software (GPL) (2018).
- [31] L. E. Kidder, C. M. Will, and A. G. Wiseman, *Phys. Rev. D* **47**, 4183 (1993), arXiv:gr-qc/9211025.
- [32] L. E. Kidder, *Phys. Rev. D* **52**, 821 (1995), arXiv:gr-qc/9506022.
- [33] P. Ajith *et al.*, *Phys. Rev. Lett.* **106**, 241101 (2011), arXiv:0909.2867 [gr-qc].
- [34] R. Abbott *et al.* (LIGO Scientific, Virgo), (2020), arXiv:2010.14527 [gr-qc].
- [35] B. Zackay, L. Dai, and T. Venumadhav, (2018), arXiv:1806.08792 [astro-ph.IM].
- [36] B. Zackay, T. Venumadhav, J. Roulet, L. Dai, and M. Zaldarriaga, (2019), arXiv:1908.05644 [astro-ph.IM].
- [37] F. Feroz and M. P. Hobson, *Mon. Not. Roy. Astron. Soc.* **384**, 449 (2008), arXiv:0704.3704 [astro-ph].
- [38] F. Feroz, M. P. Hobson, and M. Bridges, *Mon. Not. Roy. Astron. Soc.* **398**, 1601 (2009), arXiv:0809.3437 [astro-ph].
- [39] J. Buchner, A. Georgakakis, K. Nandra, L. Hsu, C. Rangel, M. Brightman, A. Merloni, M. Salvato, J. Donley, and D. Kocevski, *Astronomy & Astrophysics* **564**, A125 (2014).
- [40] P. A. R. Ade *et al.* (Planck), *Astron. Astrophys.* **594**, A13 (2016), arXiv:1502.01589 [astro-ph.CO].
- [41] L. Blanchet, *Living Rev. Rel.* **17**, 2 (2014), arXiv:1310.1528 [gr-qc].
- [42] L. E. Kidder, *Phys. Rev. D* **77**, 044016 (2008), arXiv:0710.0614 [gr-qc].
- [43] E. Berti, V. Cardoso, J. A. Gonzalez, U. Sperhake, M. Hannam, S. Husa, and B. Bruegmann, *Phys. Rev. D* **76**, 064034 (2007), arXiv:gr-qc/0703053.
- [44] L. Blanchet, G. Faye, B. R. Iyer, and S. Sinha, *Class. Quant. Grav.* **25**, 165003 (2008), [Erratum: *Class. Quant. Grav.* **29**, 239501 (2012)], arXiv:0802.1249 [gr-qc].
- [45] J. Roulet *et al.*, *to appear* (2021).
- [46] B. Farr, E. Ochsner, W. M. Farr, and R. O’Shaughnessy, *Phys. Rev. D* **90**, 024018 (2014), arXiv:1404.7070 [gr-qc].
- [47] Y. Huang, C.-J. Haster, S. Vitale, A. Zimmerman, J. Roulet, T. Venumadhav, B. Zackay, L. Dai, and M. Zaldarriaga, *Phys. Rev. D* **102**, 103024 (2020), arXiv:2003.04513 [gr-qc].
- [48] A. H. Nitz and C. D. Capano, *Astrophys. J. Lett.* **907**,

- L9 (2021), arXiv:2010.12558 [astro-ph.HE].
- [49] S. Olsen *et al.*, *to appear* (2021).
- [50] R. Abbott *et al.* (LIGO Scientific, Virgo), *Phys. Rev. Lett.* **125**, 101102 (2020), arXiv:2009.01075 [gr-qc].
- [51] C. Cutler and E. E. Flanagan, *Phys. Rev. D* **49**, 2658 (1994), arXiv:gr-qc/9402014.
- [52] E. Poisson and C. M. Will, *Phys. Rev. D* **52**, 848 (1995), arXiv:gr-qc/9502040.
- [53] E. Baird, S. Fairhurst, M. Hannam, and P. Murphy, *Phys. Rev. D* **87**, 024035 (2013), arXiv:1211.0546 [gr-qc].
- [54] R. Abbott *et al.* (LIGO Scientific, Virgo), *Phys. Rev. D* **102**, 043015 (2020), arXiv:2004.08342 [astro-ph.HE].
- [55] R. Abbott *et al.* (LIGO Scientific, Virgo), *Astrophys. J. Lett.* **896**, L44 (2020), arXiv:2006.12611 [astro-ph.HE].
- [56] B. Paczynski, in *Structure and Evolution of Close Binary Systems*, Vol. 73, edited by P. Eggleton, S. Mitton, and J. Whelan (1976) p. 75.
- [57] E. P. J. van den Heuvel, in *Structure and Evolution of Close Binary Systems*, Vol. 73, edited by P. Eggleton, S. Mitton, and J. Whelan (1976) p. 35.
- [58] A. V. Tutukov and L. R. YungelSon, *Monthly Notices of the Royal Astronomical Society* **260**, 675 (1993).
- [59] K. A. Postnov and L. R. Yungelson, *Living Rev. Rel.* **17**, 3 (2014), arXiv:1403.4754 [astro-ph.HE].
- [60] S. F. Portegies Zwart and S. McMillan, *Astrophys. J. Lett.* **528**, L17 (2000), arXiv:astro-ph/9910061.
- [61] J. M. B. Downing, M. J. Benacquista, M. Giersz, and R. Spurzem, *Monthly Notices of the Royal Astronomical Society* **407**, 1946 (2010).
- [62] C. L. Rodriguez, M. Morscher, B. Pattabiraman, S. Chatterjee, C.-J. Haster, and F. A. Rasio, *Phys. Rev. Lett.* **115**, 051101 (2015), [Erratum: *Phys. Rev. Lett.* **116**, 029901 (2016)], arXiv:1505.00792 [astro-ph.HE].
- [63] F. Antonini and F. A. Rasio, *Astrophys. J.* **831**, 187 (2016), arXiv:1606.04889 [astro-ph.HE].
- [64] B. M. Ziosi, M. Mapelli, M. Branchesi, and G. Tormen, *Mon. Not. Roy. Astron. Soc.* **441**, 3703 (2014), arXiv:1404.7147 [astro-ph.GA].
- [65] S. Banerjee, *Mon. Not. Roy. Astron. Soc.* **481**, 5123 (2018), arXiv:1805.06466 [astro-ph.HE].
- [66] J. Kumamoto, M. S. Fujii, and A. Tanikawa, *Mon. Not. Roy. Astron. Soc.* **486**, 3942 (2019), arXiv:1811.06726 [astro-ph.HE].
- [67] M. Dominik, K. Belczynski, C. Fryer, D. Holz, E. Berti, T. Bulik, I. Mandel, and R. O’Shaughnessy, *Astrophys. J.* **759**, 52 (2012), arXiv:1202.4901 [astro-ph.HE].
- [68] J. J. Eldridge and E. R. Stanway, *Mon. Not. Roy. Astron. Soc.* **462**, 3302 (2016), arXiv:1602.03790 [astro-ph.HE].
- [69] S. E. de Mink and I. Mandel, *Mon. Not. Roy. Astron. Soc.* **460**, 3545 (2016), arXiv:1603.02291 [astro-ph.HE].
- [70] C. L. Rodriguez, S. Chatterjee, and F. A. Rasio, *Phys. Rev. D* **93**, 084029 (2016), arXiv:1602.02444 [astro-ph.HE].
- [71] M. Spera, M. Mapelli, N. Giacobbo, A. A. Trani, A. Bressan, and G. Costa, *Monthly Notices of the Royal Astronomical Society* **485**, 889 (2019).
- [72] C. J. Neijssel, A. Vigna-Gómez, S. Stevenson, J. W. Barrett, S. M. Gaebel, F. Broekgaarden, S. E. de Mink, D. Szécsi, S. Vinciguerra, and I. Mandel, *Mon. Not. Roy. Astron. Soc.* **490**, 3740 (2019), arXiv:1906.08136 [astro-ph.SR].
- [73] J. M. Lattimer, *Ann. Rev. Nucl. Part. Sci.* **62**, 485 (2012), arXiv:1305.3510 [nucl-th].
- [74] F. Özel and P. Freire, *Ann. Rev. Astron. Astrophys.* **54**, 401 (2016), arXiv:1603.02698 [astro-ph.HE].
- [75] A. Nathanail, E. R. Most, and L. Rezzolla, *Astrophys. J. Lett.* **908**, L28 (2021), arXiv:2101.01735 [astro-ph.HE].
- [76] H.-T. Janka, *Ann. Rev. Nucl. Part. Sci.* **62**, 407 (2012), arXiv:1206.2503 [astro-ph.SR].
- [77] C. L. Fryer, K. Belczynski, G. Wiktorowicz, M. Dominik, V. Kalogera, and D. E. Holz, *Astrophys. J.* **749**, 91 (2012), arXiv:1110.1726 [astro-ph.SR].
- [78] E. R. Most, L. J. Papenfort, L. R. Weih, and L. Rezzolla, *Mon. Not. Roy. Astron. Soc.* **499**, L82 (2020), arXiv:2006.14601 [astro-ph.HE].
- [79] I. A. Rather, A. A. Usmani, and S. K. Patra, (2020), arXiv:2011.14077 [nucl-th].
- [80] I. A. Rather, U. Rahaman, M. Imran, H. C. Das, A. A. Usmani, and S. K. Patra, (2021), arXiv:2102.04067 [nucl-th].
- [81] W. M. Farr, S. Stevenson, M. Coleman Miller, I. Mandel, B. Farr, and A. Vecchio, *Nature* **548**, 426 (2017), arXiv:1706.01385 [astro-ph.HE].
- [82] C. L. Rodriguez, M. Zevin, C. Pankow, V. Kalogera, and F. A. Rasio, *Astrophys. J. Lett.* **832**, L2 (2016), arXiv:1609.05916 [astro-ph.HE].
- [83] K. Belczynski *et al.*, *Astron. Astrophys.* **636**, A104 (2020), arXiv:1706.07053 [astro-ph.HE].
- [84] J. Fuller and L. Ma, *Astrophys. J. Lett.* **881**, L1 (2019), arXiv:1907.03714 [astro-ph.SR].
- [85] J. Fuller, A. L. Piro, and A. S. Jermyn, *Monthly Notices of the Royal Astronomical Society* **485**, 3661 (2019).
- [86] I. Mandel and S. E. de Mink, *Mon. Not. Roy. Astron. Soc.* **458**, 2634 (2016), arXiv:1601.00007 [astro-ph.HE].
- [87] P. Marchant, N. Langer, P. Podsiadlowski, T. M. Tauris, and T. J. Moriya, *Astron. Astrophys.* **588**, A50 (2016), arXiv:1601.03718 [astro-ph.SR].
- [88] V. Kalogera, *Astrophys. J.* **541**, 319 (2000), arXiv:astro-ph/9911417.
- [89] B. Willems, M. Henninger, T. Levin, N. Ivanova, V. Kalogera, F. X. Timmes, and C. L. Fryer, *Astrophys. J.* **625**, 324 (2005), arXiv:astro-ph/0411423.
- [90] D. Gerosa and E. Berti, *Phys. Rev. D* **95**, 124046 (2017), arXiv:1703.06223 [gr-qc].
- [91] Z. Doctor, D. Wysocki, R. O’Shaughnessy, D. E. Holz, and B. Farr, *The Astrophysical Journal* **893**, 35 (2020).
- [92] C. L. Rodriguez, M. Zevin, P. Amaro-Seoane, S. Chatterjee, K. Kremer, F. A. Rasio, and C. S. Ye, *Phys. Rev. D* **100**, 043027 (2019), arXiv:1906.10260 [astro-ph.HE].
- [93] F. Pretorius, *Phys. Rev. Lett.* **95**, 121101 (2005), arXiv:gr-qc/0507014.
- [94] M. A. Scheel, M. Boyle, T. Chu, L. E. Kidder, K. D. Matthews, and H. P. Pfeiffer, *Phys. Rev. D* **79**, 024003 (2009), arXiv:0810.1767 [gr-qc].
- [95] M. Fishbach, D. E. Holz, and B. Farr, *Astrophys. J. Lett.* **840**, L24 (2017), arXiv:1703.06869 [astro-ph.HE].
- [96] F. Hofmann, E. Barausse, and L. Rezzolla, *Astrophys. J. Lett.* **825**, L19 (2016), arXiv:1605.01938 [gr-qc].
- [97] X. Jiménez-Forteza, D. Keitel, S. Husa, M. Hannam, S. Khan, and M. Pürrer, *Phys. Rev. D* **95**, 064024 (2017), arXiv:1611.00332 [gr-qc].
- [98] C.-M. Deng, *Mon. Not. Roy. Astron. Soc.* **497**, 643 (2020), arXiv:2007.02744 [astro-ph.HE].
- [99] M. Fishbach and D. E. Holz, *The Astrophysical Journal* **851**, L25 (2017).

- [100] J. Roulet and M. Zaldarriaga, *Mon. Not. Roy. Astron. Soc.* **484**, 4216 (2019), arXiv:1806.10610 [astro-ph.HE].
- [101] B. Liu and D. Lai, *Mon. Not. Roy. Astron. Soc.* **502**, 2049 (2021), arXiv:2009.10068 [astro-ph.HE].
- [102] M. Zevin, S. S. Bavera, C. P. L. Berry, V. Kalogera, T. Fragos, P. Marchant, C. L. Rodriguez, F. Antonini, D. E. Holz, and C. Pankow, *Astrophys. J.* **910**, 152 (2021), arXiv:2011.10057 [astro-ph.HE].
- [103] V. Varma and P. Ajith, *Phys. Rev. D* **96**, 124024 (2017), arXiv:1612.05608 [gr-qc].
- [104] J. Calderón Bustillo, S. Husa, A. M. Sintes, and M. Pürrer, *Phys. Rev. D* **93**, 084019 (2016), arXiv:1511.02060 [gr-qc].
- [105] F. H. Shaik, J. Lange, S. E. Field, R. O’Shaughnessy, V. Varma, L. E. Kidder, H. P. Pfeiffer, and D. Wysocki, *Phys. Rev. D* **101**, 124054 (2020), arXiv:1911.02693 [gr-qc].